Radiation Hardness of MALTA2, a Monolithic Active Pixel Sensor for Tracking Applications

D. V. Berlea, P. Allport, I. Asensi Tortajada, D. Bortoletto, C. Buttar, E. Charbon, *Fellow, IEEE*, F. Dachs, V. Dao, H. Denizili, D. Dobrijevic, L. Flores Sanz de Acedo, A. Gabrielli, M. Gazi, L. Gonella, V. Gonzalez, *Senior Member, IEEE*, G. Gustavino, M. LeBlanc, K. Y. Oyulmaz, H. Pernegger, F. Piro, *Graduate Student Member, IEEE*, P. Riedler, M. van Rijnbach, H. Sandaker, A. Sharma, W. Snoeys, *Senior Member, IEEE*, C. A. Solans Sanchez, T. Suligoj, *Member, IEEE*, M. Vazquez Nunez, J. Weick, S. Worm, and A. M. Zoubir, *Life Fellow, IEEE*

***Abstract*— MALTA is a depleted monolithic active pixel sensor (DMAPS) developed in the Tower Semiconductor 180-nm CMOS imaging process. Monolithic CMOS sensors offer advantages over current hybrid imaging sensors in terms of both increased tracking performance due to lower material budget and ease of integration and construction costs due to the integration of read-out and active sensor into one ASIC. Current research and development efforts are aimed toward radiation hard designs up to 100 Mrad in total ionizing dose (TID) and 1×10^{15} 1 MeV n_{eq}/cm^2 in nonionizing energy loss (NIEL). The design of the MALTA sensors was specifically chosen to achieve radiation hardness up to these requirements and satisfy current and future collider constraints. The current MALTA pixel architecture uses small electrodes which provide less noise, higher signal voltage, and a better power-to-performance ratio. To counteract the loss of efficiency in pixel corners, modifications to the Tower process have been implemented. The MALTA sensors have been tested during the 2021 and 2022 SPS CERN Test Beam in the MALTA telescope. The telescope ran for the whole duration of the beam time and took data to characterize the novel MALTA2 variant and the performance of irradiated samples in terms of efficiency and cluster size. These campaigns show that MALTA is an interesting prospect for HL-LHC and beyond collider experiments, providing both very good tracking capabilities and radiation hardness in harsh radiation environments.**

***Index Terms*— CMOS, MAPS, radiation damage, silicon, tracking.**

Manuscript received 30 April 2023; revised 15 August 2023 and 5 September 2023; accepted 6 September 2023. Date of publication 11 September 2023; date of current version 24 October 2023. This work was supported by the European Unions Horizon 2020 Research and Innovation Programme under Grant 101004761 (AIDAinnova), Grant 675587 (STREAM), and Grant 654168 (AIDA-2020).

D. V. Berlea and S. Worm are with Deutsches Elektronen-Synchrotron DESY, 15738 Zeuthen, Germany, and also with the Humboldt University Berlin, 10117 Berlin, Germany (e-mail: vlad.berlea@desy.de; steven.worm@desy.de).

P. Allport and L. Gonella are with the Department of Physics and Astronomy, University of Birmingham, B15 2TT Birmingham, U.K. (e-mail: allport@cern.ch; laura.gonella@cern.ch).

I. Asensi Tortajada, F. Dachs, V. Dao, D. Dobrijevic, L. Flores Sanz de Acedo, A. Gabrielli, G. Gustavino, M. LeBlanc, H. Pernegger, F. Piro, P. Riedler, , M. van Rijnbach, A. Sharma, W. Snoeys, C. A. Solans Sanchez, M. Vazquez Nunez, and J. Weick are with the CERN Experimental Physics Department, 1211 Geneva, Switzerland (e-mail: ignacio.asensi@cern.ch; florian.dachs@cern.ch; valerio.dao@cern.ch; dominik.dobrijevic@cern.ch; leyre.flores@cern.ch; andrea.gabrielli@cern.ch; giuliano.gustavino@cern.ch; matt.leblanch@cern.ch; heinz.pernegger@cern.ch; francesco.piro@cern.ch; petra.riedler@cern.ch; milou.van.rijnbach@cern.ch; abhishek.sharma@cern.ch; walter.snoeys@cern.ch; carlos.solans@cern.ch; marcos.vazquez.nunez@cern.ch; julian.weick@cern.ch).

D. Bortoletto and M. Gazi are with the Department of Particle Physics, University of Oxford, OX1 3AZ Oxford, U.K. (e-mail: daniela.bortoletto@physics.ox.ac.uk; martin.gazi@cern.ch).

C. Buttar is with the Faculty of Physics and Astronomy, University of Glasgow, G12 8QQ Glasgow, U.K. (e-mail: craig.buttar@glasgow.ac.uk).

E. Charbon is with the Advanced Quantum Architecture Laboratory (AQUA), Ecole Polytechnique Fé dérale de Lausanne, 1015 Lausanne, Switzerland (e-mail: edoardo.charbon@epfl.ch).

H. Denizili and K. Y. Oyulmaz are with the Department of Physics, Bolu Abant Izzet Baysal University, 14030 Bolu, Turkey (e-mail: haluk.denizli@cern.ch; kaan.yuksel.oyulmaz@cern.ch).

V. Gonzalez is with the University of Valencia, 46010 Valencia, Spain (e-mail: vicente.gonzalez@uv.es).

H. Sandaker is with the Department of Physics, University of Oslo, CH-1211 Geneva, Norway (e-mail: heidi.sandaker@fys.uio.no).

T. Suligoj is with the Faculty of Electrical Engineering and Computing, University of Zagreb, 10000 Zagreb, Croatia (e-mail: tomislav.suligoj@fer.hr).

A. M. Zoubir is with the Technische Universität Darmstadt, Darmstadt, Germany (e-mail: zoubir@spg.tu-darmstadt.de).

Color versions of one or more figures in this article are available at https://doi.org/10.1109/TNS.2023.3313721.

Digital Object Identifier 10.1109/TNS.2023.3313721

I. Introduction

CURRENT and future collider experiments have enjoyed constant improvements in terms of center-of-mass energy and luminosity [1]. To cope with increasingly harsh requirements for the detecting systems used by high-energy physics collider experiments, continuous research and development in the instrumentation field is pursued to produce better performing systems [2]. This challenge is further amplified for the inner trackers, which reside at the inner radii of these experiments. Currently, most pixel trackers are formed from hybrid modules; a sensor bump bonded to an ASIC. While the result is a robust, radiation hard tracking detector, it comes with several disadvantages, such as expensive bump bonding procedure, large material budget, high power consumption, and large pixel pitches. An emerging alternative to the hybrid tracking sensor is the small collection electrode, depleted monolithic active pixel sensor (DMAPS). DMAPSs offer a lot of advantages, such as low material budget, low power consumption, high signal-to-noise ratio, and lower pixel pitches.

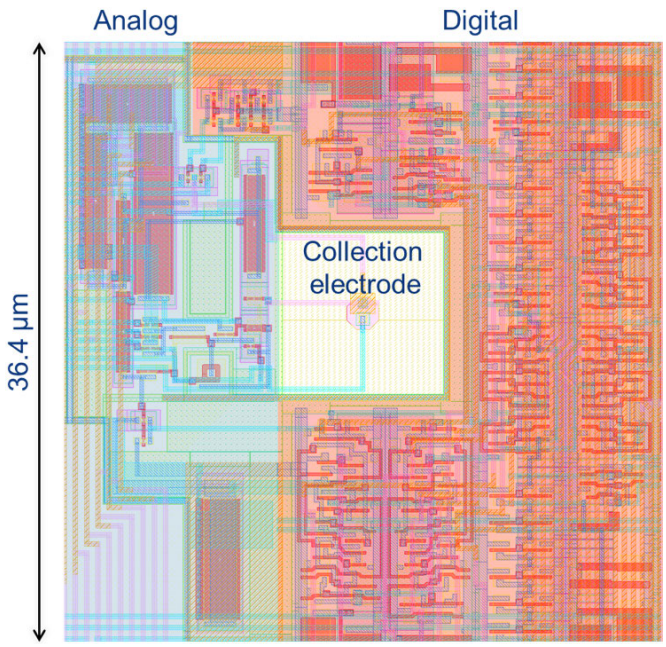

Fig. 1. MALTA pixel with small charge collection electrode.

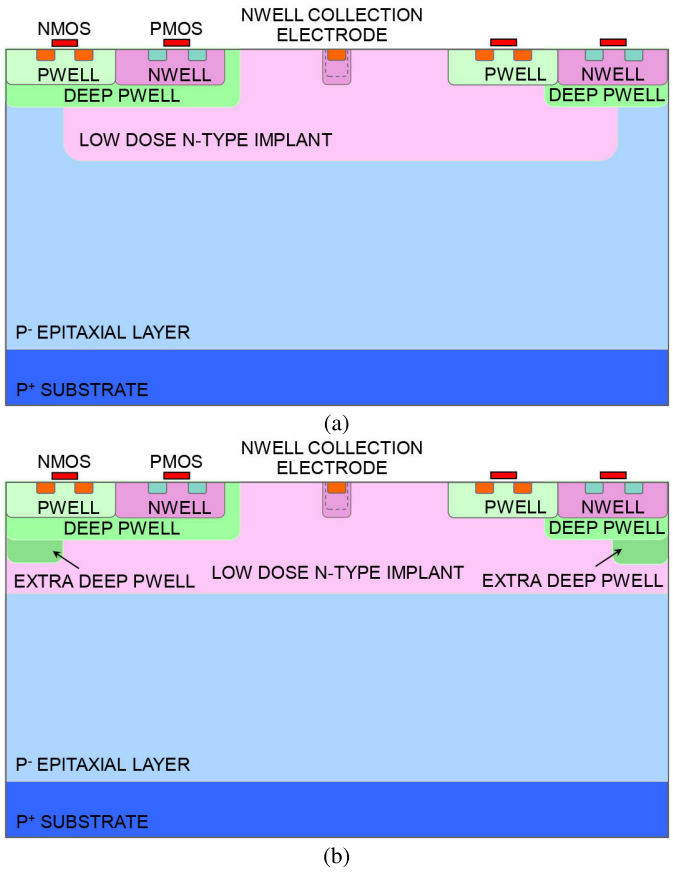

Fig. 2. Cross section of the modified process, implementing a small electrode pixel. The n-blanket extends the junction to the full pixel size. Two variations of this process are presented. (a) Modified process where the low-dose n-implant is removed at the edge of the pixel (NGAP). (b) Extra deep p-well is added at the edge of the pixel (XDPW).

Improvements in foundry processes and pixel architectures push the viability of this technology for harsher radiation environments [3]. Currently, radiation hardness remains one of the main hurdles for the mass adoption of DMAPS in most high-energy physics experiments, and hence, it remains one of the most important figures of merit for tracking detector research and development.

II. The MALTA Sensor Family

MALTA is a small collection electrode DMAPS fabricated by Tower in a 180-nm feature size process [4]. It has an active matrix of 512 × 512 pixels with a pixel pitch of 36.4 × 36.4 μm^2 and an active area of 18.3 × 18.3 mm^2. The hexagonal small collection electrode (3 μm) in the pixel center as seen in Fig. 1 provides a very small capacitance (5 fF), low power consumption (1 μW/pixel) [5], and a large signal-to-noise ratio. Lateral depletion of the pixel is achieved via a low-dose n-type layer in the modified Tower process [6]. To combat efficiency losses in the pixel corners [7] caused by electric potential minima, two further process modifications have been made: a gap in the n-layer (NGAP), Fig. 2(a) and an extra deep highly doped p-well implant (XDPW), Fig. 2(b). Both the modifications serve the same purpose of enhancing the lateral field as suggested by TCAD simulations [8], and thus mitigate efficiency losses in irradiated samples. MALTA sensors are fabricated on epitaxial (Epi) (25- or 30-μm thickness) and Czochralski (Cz) substrates (100, 300-μm thickness). MALTA-Cz's thicker detection layer enhances the total collected charge produced by a minimum ionizing particle (that leads to the minimum amount of ionization in a substrate in its path) from 1500 e$^-$ for Epi substrates to more than 6000 e$^-$. A proportional increase in the front-end voltage step is expected and a more compact open-loop amplification method is available, lowering the analog circuit size.

To cope with high hit rates and also lower the sensor power consumption, a dedicated asynchronous read-out architecture has been developed [9], without the need for propagating a clock across the matrix. Charge generated in the silicon bulk leads to the generation of a voltage step through the charge collection electrode capacitance that is then passed to a discriminator with a global threshold setting. The sense node is reset with a diode reset (inherited also by MALTA2) or a P-MOSFET. Pixels are grouped in 2 × 8 groups so that all the hits in a group within a 5-ns time window are read out at once. Whenever a pixel generates a signal above threshold, a group of 16 pixels trigger the readout and the output of every other group is routed toward a double-column read-out (Fig. 3). In addition, five reference bits are routed out to distinguish between different pixel groups.

III. MALTA2

MALTA2 is the second generation of Tower 180-nm DMAPS. It is approximately half the size of the MALTA sensor, with an active area of 224 × 512 pixels (18.33 mm^2). MALTA2 inherits the asynchronous readout and provides slow control improvements and an improved front-end, first tested in

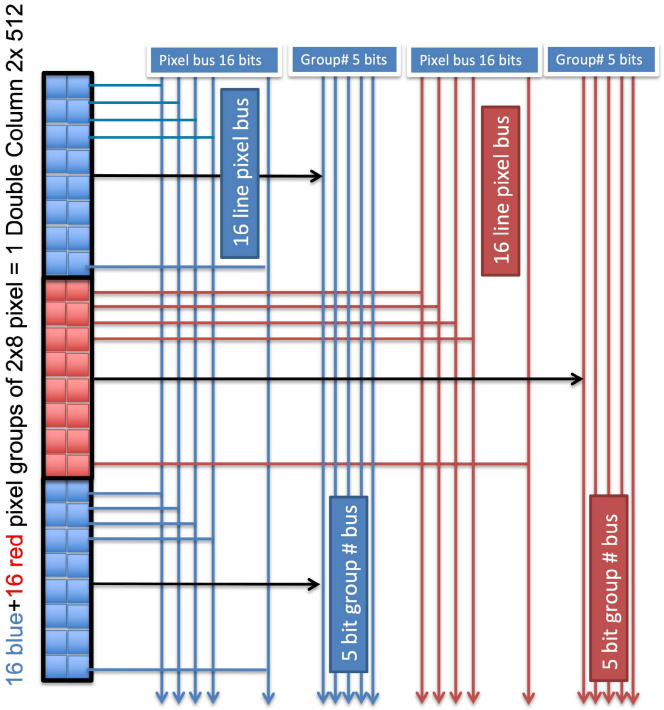

Fig. 3. Asynchronous double-column MALTA readout architecture. "Odd" 16 pixel groups are read out through the blue bus, and "even" 16 pixel groups are read out through the red bus. Also, five reference bits are also routed out to distinguish different pixel groups.

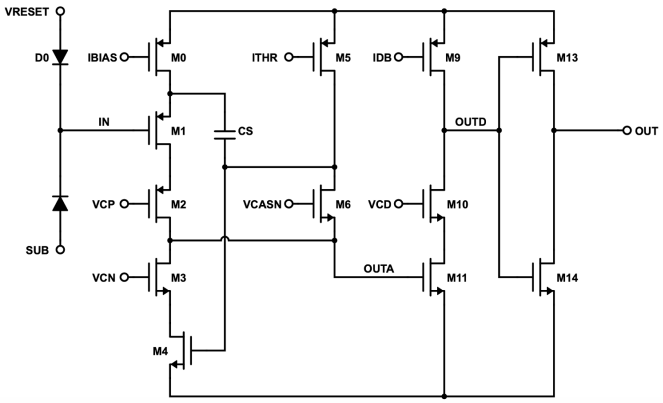

Fig. 4. MALTA cascode analog front-end.

the mini-MALTA demonstrator [10]. As can be seen in Fig. 4, the new front-end adds a cascoded stage in the input branch and enlarged transistors in the amplifier feedback loop. This increases the gain and lowers the noise, lowering the operational threshold from 200 to ∼100 e⁻.

A. Threshold and Noise

The threshold of MALTA2 can be measured with an in-pixel charge injection test capacitance (∼300 aF). The pixel threshold is measured as the 50%-occupancy point of the hit occupancy (number of times a hit is generated by an injected charge) versus injected charge "*S*-curve." Fig. 5(a) showcases the normalized threshold distribution for MALTA and MALTA2 in configurations providing similar threshold. Similar threshold distribution is observed in both the sensors,

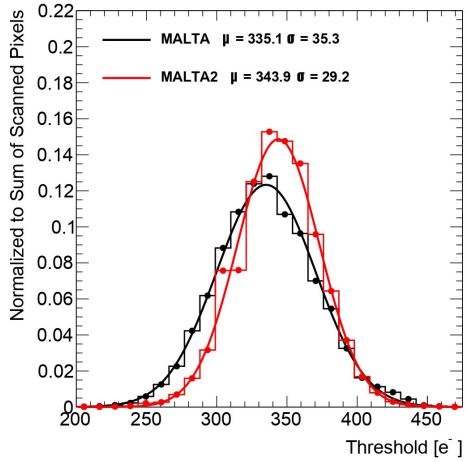

(a)

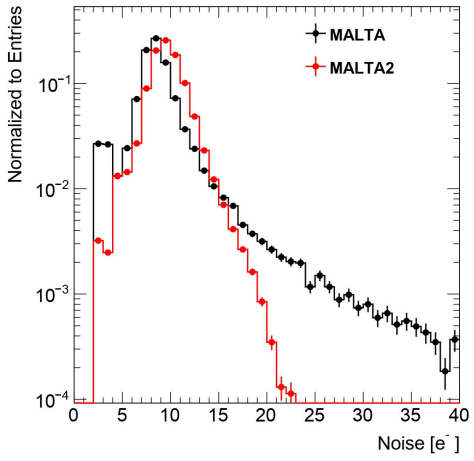

(b)

Fig. 5. (a) Threshold and (b) noise distributions for MALTA (black curve) and MALTA2 (red curve) samples. The rms values of the noise distributions are around 3.5 and 2.25 for MALTA and MALTA2, respectively.

achieving an expected 10% threshold dispersion from the mean. The improvement in the front-end brought on by MALTA2 can be seen in the normalized noise distribution in Fig. 5(b). One of the benefits of the cascoded stage and the enlarged transistors is a diminished random telegraph signal (RTS). The benefits of the new front-end are both the drop in the non-Gaussian noise tail and additional radiation hardness (showcased already by the mini-MALTA small demonstrator [11]).

B. Test Beam Results With MALTA2

To characterize the novel MALTA2 samples in terms of efficiency, cluster size, and timing, the MALTA telescope in the SPS test beam area has been used [12]. It consists of six MALTA tracking planes that provide track reconstruction and a trigger for the DUTs (up to two DUTs inside a temperature- and humidity-controlled cold box) and a scintillator for timing reference. All the samples have been characterized with a 180-GeV hadron beam.

Fig. 6 shows the efficiency of the nonirradiated MALTA2 full matrix. A uniform efficiency larger than 99.6% is observed over the entire matrix. The cluster size for multiple threshold

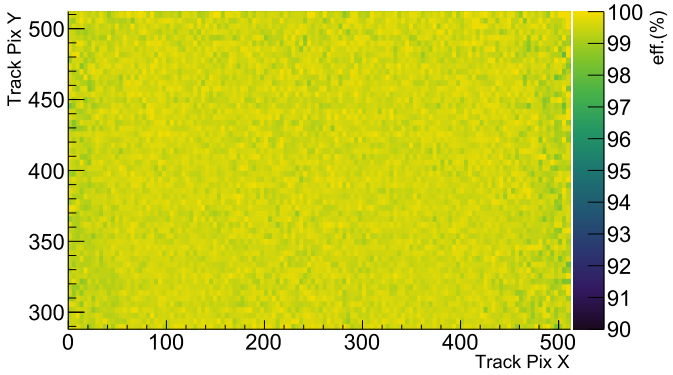

Fig. 6. Two-dimensional efficiency map of the entire matrix of nonirradiated MALTA2 (Cz, NGAP, 300 − μm-thick, high doping of n-blanket), at −6-V SUB bias and −6-V PWELL bias. Threshold corresponds to 150 electrons. A uniform efficiency of 99.6% was achieved for the entire matrix.

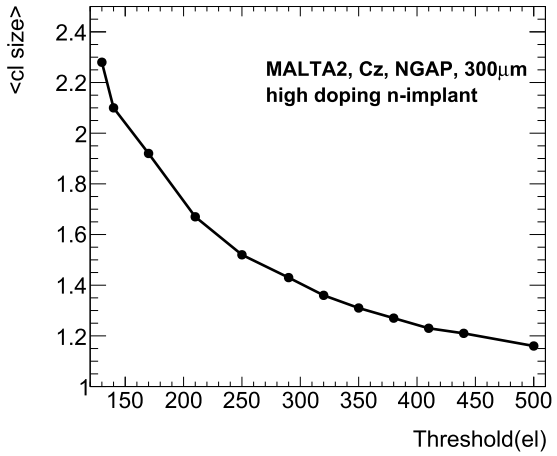

Fig. 7. Average cluster size of nonirradiated MALTA2 (Cz, NGAP, 300 − μm-thick, high doping of n-blanket) versus the threshold in electrons, at −6-V SUB bias and −6-V PWELL bias.

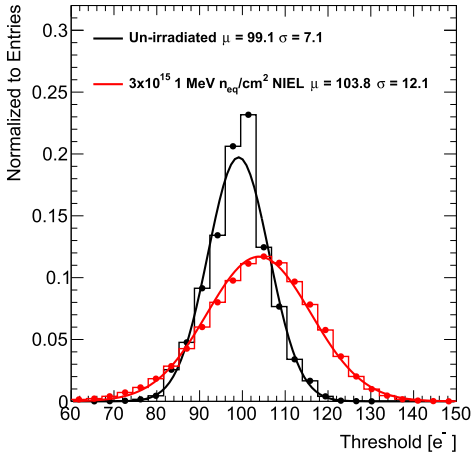

Fig. 8. Threshold distributions of MALTA2 samples before and after neutron irradiation at 3×10^{15} 1 MeV n_{eq}/cm^2. The threshold scans are obtained for the lowest threshold configuration achievable in that sensor.

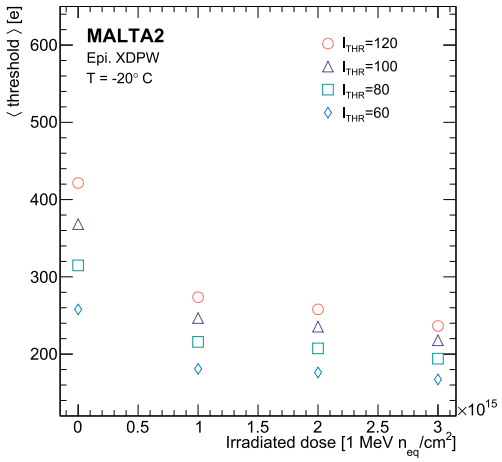

Fig. 9. Average threshold value of MALTA2 sensors versus the irradiated dose for several configurations.

configurations of a MALTA2 sample is presented in Fig. 7. An increase in cluster size can be seen for lower thresholds, as diffused charged has a higher impact on the reconstructed clusters.

The timing properties of the MALTA2 sensor have been studied in [13]. A timing resolution that includes the effects on the entire read out chain have been determined for both an Epi sample, 1.9 ns, and a Cz sample, 1.8 ns.

IV. Radiation Tolerance of MALTA2

The radiation hardness of MALTA2 samples has been tested in terms of both the NIEL-induced displacement damage (DD) and ionizing effects (TID). Unbiased samples have been irradiated at the TRIGA reactor in Ljubljana [14] up to 3×10^{15} 1 MeV n_{eq}/cm^2 with an approximate neutron flux of 10^{12} $cm^{-2}s^{-1}$. Another sample was irradiated with X rays (50-keV energy, a tungsten target, and a dose rate of 1 Mrad/h) while biased at −6-V SUB and −6-V PWELL up to 150 Mrad. To minimize annealing effects, all the samples have been stored and tested at −20 °C and low humidity. The low temperature also helps contain the increase in leakage current. Due to the low power dissipation of the sensor, a low temperature can be maintained on the sensor during its application as a tracker.

A. Threshold and Noise Degradation

As the operation at low threshold is important in a high radiation environment, a thorough study on the threshold dependence on radiation dose has been performed on MALTA2 [15]. Fig. 8 highlights the lowest sensor threshold that can be applied on a MALTA2 sample at no irradiation and after 3×10^{15} 1 MeV n_{eq}/cm^2. The sensor can still be operated at low thresholds after a high irradiation dose and the threshold dispersion is close to 10%. The change in the threshold configuration with the NIEL dose is shown in Fig. 9. The drop in threshold (for a certain sensor configuration) at higher radiation doses is not expected to be induced by damage in the FE, but due to the change in capacitance of the substrate, which in turn leads to a change in the sensor's gain [11]. At high NIEL doses, the Shockley–Read–Hall (SRH) carrier removal effect becomes efficient and can induce doping concentration modifications in the n-bulk layer [16].

Radiation damage in the silicon bulk induces charge generation centers that through a nonradiative recombination mechanism is expected to contribute to the increase in the

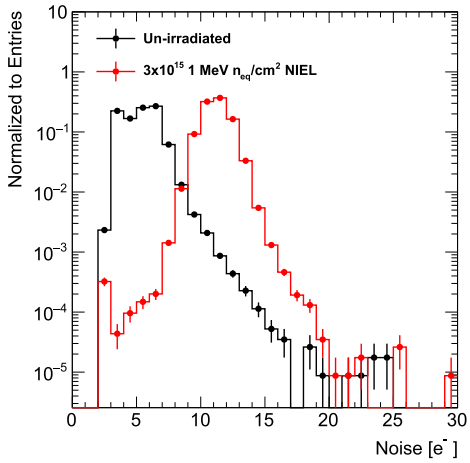

Fig. 10. Noise distributions of MALTA2 samples before and after neutron irradiation at 3×10^{15} 1 MeV n_{eq}/cm^2.

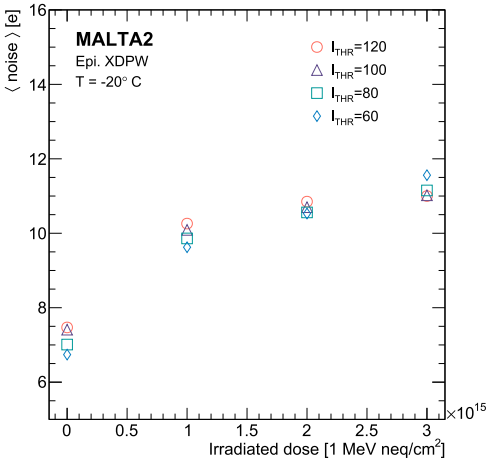

Fig. 11. Average noise level of MALTA2 sensors versus the irradiated dose for several configurations.

sensor leakage current. Fig. 10 shows the elevated noise at 3×10^{15} 1 MeV n_{eq}/cm^2. No significant non-Gaussian component is observed in the noise distribution, indicating no contribution from RTS to the total noise. The increase in noise with radiation dose is presented in Fig. 11. A small-signal ac noise analysis [15] performed on the FE showed that before irradiation, the dominating noise contribution (thermal noise) comes from the amplifying circuitry. This is expected to remain the same after irradiation, assuming a similar effect on all the active FE elements. Even for the highest irradiation dose, a threshold-to-noise ratio higher than 10 is achieved.

Trapped charge in the oxide induced by TID shifts the operating point of MOSFETs in the front-end. Fig. 12 illustrates the impact of TID on the threshold. A large drop in threshold can be seen (red points) for a constant sensor configuration, for TID values higher than 1 Mrad. This is a feature of the used technology node and can be corrected, by tuning the DAC configuration (blue points). An increase in noise has also been observed at elevated TID values [17].

B. Efficiency and Cluster Size Degradation

1) *Neutron irradiation* is expected to degrade the efficiency and cluster size of MALTA2 sensors. Point-like and

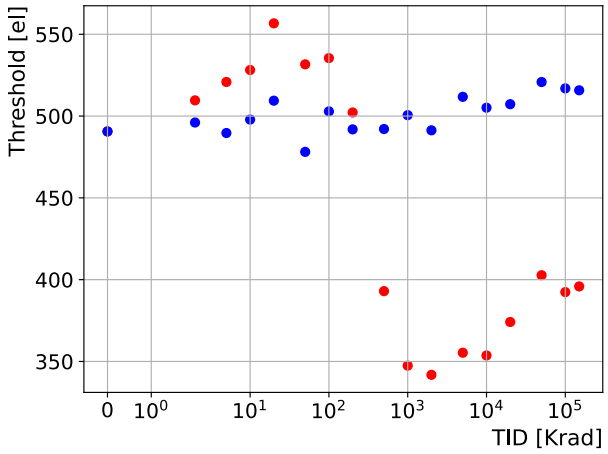

Fig. 12. Threshold behavior of MALTA2 over a TID range of 0 krad to 150 Mrad. Red dots show the behavior of a constant DAC configuration, while blue dots show the result of a constant manual readjustment of the front-end parameters.

clusters of displaced lattice atoms lower the charge collection efficiency through trap-assisted recombination effects. The recombination of generated charge is enhanced in the electric potential minima regions of the pixel, such as the pixel corners. MALTA2 directly addresses these concerns in the pixel design (low doping n-layer and NGAP/XDPW modifications), but elevated NIEL doses lead to carrier removal effects, which in turn limits the extent of depletion volume.

Cz MALTA2 samples have been irradiated with neutrons up to 3×10^{15} 1 MeV n_{eq}/cm^2. Due to the lack of backside metallization, a conductive glue was applied on the backside to propagate the substrate voltage across the whole sensor. Some inefficient regions have been observed that match trapped air bubble patterns detected in the glue. Only the fiducial regions where good contact is guaranteed have been used in calculating the sensor efficiency.

Elevated substrate voltages lead to the extension of the depletion volume further into the substrate, increasing the effective volume for efficient collection of generated charge. A side affect of the elevated SUB voltage is also the increase in leakage current. The maximum voltage that can be applied to the substrate varies from chip to chip and is regulated by a compliance limit of 2 mA on the substrate current. To maintain a low enough noise in the sensor during test beam data acquisition, a balance between high SUB voltage and low threshold needs to be maintained. Fig. 13 illustrates the efficiency increase with substrate voltage [18] and threshold for various NIEL irradiation levels. At relatively low doses (1×10^{15} 1 MeV n_{eq}/cm^2), an efficiency over 98% is achieved at −10-V SUB for multiple sensor configurations. At elevated NIEL doses, the substrate voltage needs to be increased to achieve a similar depletion volume due to the carrier removal in the n-doped blanket. An efficiency of >96% is achieved for 2×10^{15} and 3×10^{15} 1 MeV n_{eq}/cm^2 at −25-V and −55-V SUB, respectively. A high efficiency

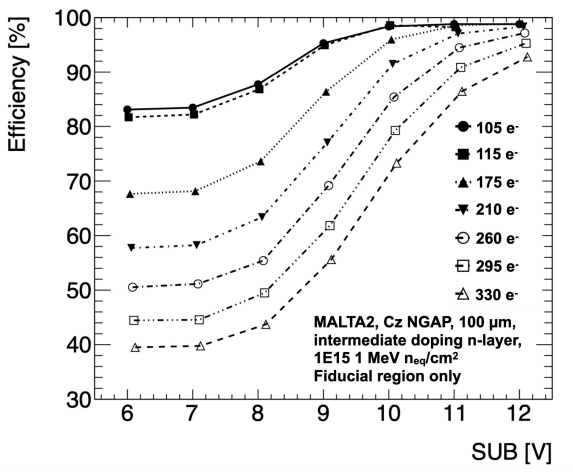

(a)

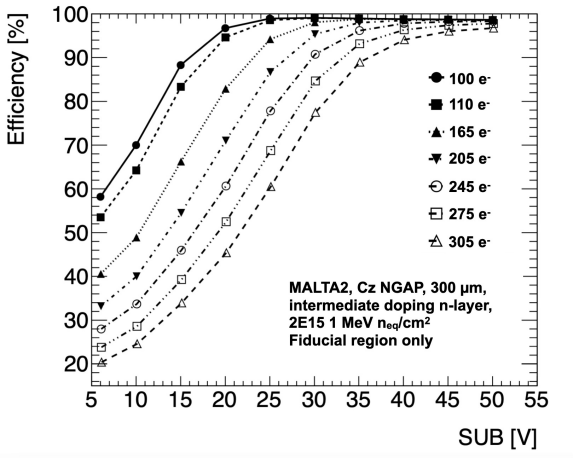

(b)

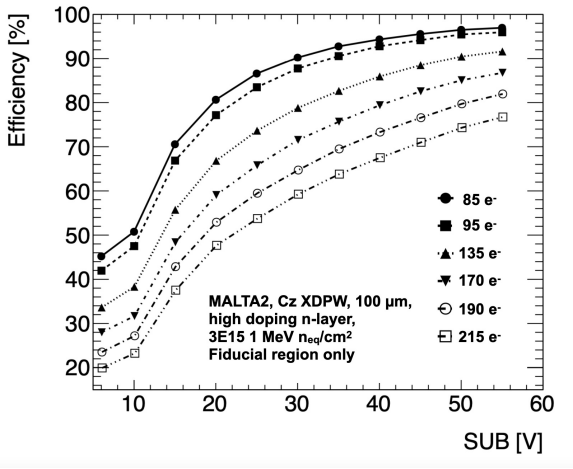

(c)

Fig. 13. Average efficiency of irradiated MALTA2 versus bias voltage at various operating threshold points and −6-V PWELL bias. Quoted efficiency corresponds to the performance in fiducial regions, where there is good electrical contact. (a) MALTA2 Cz neutron irradiated at 1×10^{15} 1 MeV n_{eq}/cm^2. Fiducial region corresponds to 10.3% of the whole array. (b) MALTA2 Cz neutron irradiated at 2×10^{15} 1 MeV n_{eq}/cm^2. Fiducial region corresponds to 9.4% of the whole array. (c) MALTA2 Cz neutron irradiated at 3×10^{15} 1 MeV n_{eq}/cm^2. Fiducial region corresponds to 4.7% of the whole array.

at 3×10^{15} 1 MeV n_{eq}/cm^2 irradiated sample was observed only in a sensor with a higher doping of the n-layer. This is most probably due to the carrier removal effect that takes place at elevated NIEL doses, which is partially canceled out by the increase in doping. The NGAP and XDPW results are comparable due to their similar effects on the sensor performance as was found during the testing of the mini-MALTA variant [11].

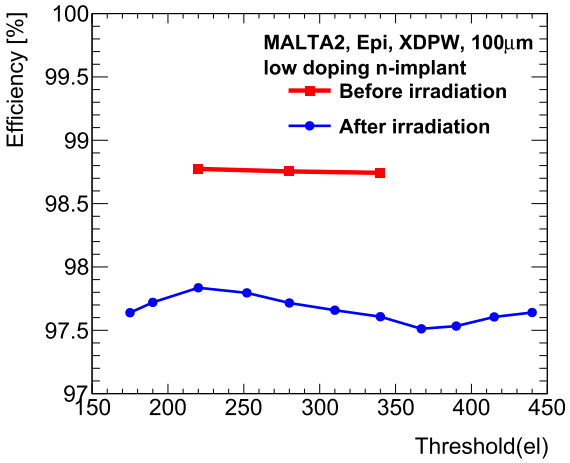

Fig. 14. Average efficiency of a MALTA2 sample versus threshold in electrons, before irradiation (red line) and after 100 Mrad X ray irradiation (blue line).

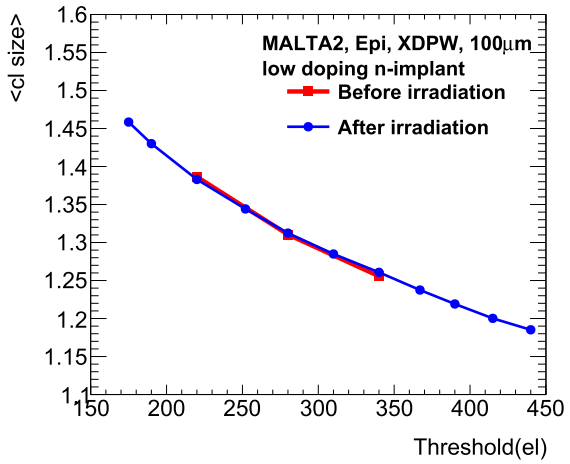

Fig. 15. Average cluster size of a MALTA2 versus threshold in electrons, before irradiation (red line) and after 100 Mrad X ray irradiation (blue line).

2) *X-ray-irradiated* MALTA2 samples up to 100 Mrad have been characterized in terms of efficiency and cluster size. Fig. 14 illustrates the efficiency in terms of threshold before and after irradiation and Fig. 15 the cluster size. For both, a drop of less than 2% is observed at the same threshold configurations, showing that TID has little impact on these variables.

V. Conclusion

MALTA2 is an attractive DMAPS for tracking applications due to its low noise and threshold, small pixel pitch, and large cluster size. Czochralski substrate samples show radiation hardness up to 3×10^{15} 1 MeV n_{eq}/cm^2 NIEL and 100 Mrad TID. Better radiation hardness has also been reached by increasing the doping of the lightly doped n-layer, which is affected by carrier removal effects at very high radiation doses. The highlighted results achieved with MALTA2 showcase the

viability of the technology for tracking at the inner radii of collider experiments.

REFERENCES

[1] I. Zurbano et al., "High-luminosity large hadron collider (HL-LHC): Technical design," CERN, Geneva, Switzerland, Tech. Rep. CERN-2020-010, Dec. 2020, doi: 10.23731/CYRM-2020-0010.

[2] M. Aleksa et al., "Strategic R&D programme on technologies for future experiments," CERN, Geneva, Switzerland, Tech. Rep. CERN-OPEN-2018-006, Dec. 2018. [Online]. Available: https://cds.cern.ch/record/2649646

[3] H. Pernegger et al., "First tests of a novel radiation hard CMOS sensor process for depleted monolithic active pixel sensors," *J. Instrum.*, vol. 12, no. 6, Jun. 2017, Art. no. P06008, doi: 10.1088/1748-0221/12/06/p06008.

[4] I. Berdalovic et al., "MALTA: A CMOS pixel sensor with asynchronous readout for the ATLAS high-luminosity upgrade," in *Proc. IEEE Nucl. Sci. Symp. Med. Imag. Conf. Proc. (NSS/MIC)*, Nov. 2018, pp. 1–4, doi: 10.1109/NSSMIC.2018.8824349.

[5] W. Snoeys, "Monolithic pixel detectors for high energy physics," *Nucl. Instrum. Methods Phys. Res. A, Accel. Spectrom. Detect. Assoc. Equip.*, vol. 731, pp. 125–130, Dec. 2013, doi: 10.1016/j.nima.2013.05.073.

[6] W. Snoeys et al., "A process modification for CMOS monolithic active pixel sensors for enhanced depletion, timing performance and radiation tolerance," *Nucl. Instrum. Methods Phys. Res. A, Accel. Spectrom. Detect. Assoc. Equip.*, vol. 871, pp. 90–96, Nov. 2017, doi: 10.1016/j.nima.2017.07.046.

[7] E. J. Schioppa et al., "Measurement results of the Malta monolithic pixel detector," *Nucl. Instrum. Methods Phys. Res. A, Accel. Spectrom. Detect. Assoc. Equip.*, vol. 958, Apr. 2020, Art. no. 162404, doi: 10.1016/j.nima.2019.162404.

[8] M. Munker et al., "Simulations of CMOS pixel sensors with a small collection electrode, improved for a faster charge collection and increased radiation tolerance," *J. Instrum.*, vol. 14, no. 5, May 2019, Art. no. C05013, doi: 10.1088/1748-0221/14/05/C05013.

[9] R. Cardella et al., "MALTA: An asynchronous readout CMOS monolithic pixel detector for the ATLAS high-luminosity upgrade," *J. Instrum.*, vol. 14, no. 6, Jun. 2019, Art. no. C05013, doi: 10.1088/1748-0221/14/06/C06019.

[10] I. A. Tortajada et al., "Latest developments and results of radiation tolerance CMOS sensors with small collection electrodes," in *Proc. JPS Conf.*, vol. 34, Feb. 2021, Art. no. 010009, doi: 10.7566/JPSCP.34.010009.

[11] M. Dyndal et al., "Mini-MALTA: Radiation hard pixel designs for small-electrode monolithic CMOS sensors for the high luminosity LHC," *J. Instrum.*, vol. 15, no. 2, Feb. 2020, Art. no. P02005, doi: 10.1088/1748-0221/15/02/P02005.

[12] M. van Rijnbach et al., "Performance of the Malta telescope," *Eur. Phys. J. C*, vol. 83, no. 7, p. 581, Jul. 2023, doi: 10.1140/epjc/s10052-023-11760-z.

[13] G. Gustavino et al., "Timing performance of radiation hard Malta monolithic pixel sensors," *J. Instrum.*, vol. 18, no. 3, Mar. 2022, Art. no. C03011.

[14] L. Snoj, G. Žerovnik, and A. Trkov, "Computational analysis of irradiation facilities at the JSI TRIGA reactor," *Appl. Radiat. Isot.*, vol. 70, no. 3, pp. 483–488, Mar. 2012, doi: 10.1016/j.apradiso.2011.11.042.

[15] F. Piro et al., "A 1-μW radiation-hard front-end in a 0.18-μm CMOS process for the MALTA2 monolithic sensor," *IEEE Trans. Nucl. Sci.*, vol. 69, no. 6, pp. 1299–1309, Jun. 2022, doi: 10.1109/TNS.2022.3170729.

[16] V. V. Kozlovski et al., "Charge carrier removal rates in n-type silicon and silicon carbide subjected to electron and proton irradiation," *Phys. B, Condens. Matter*, vol. 404, nos. 23–24, pp. 4752–4754, Dec. 2009, doi: 10.1016/j.physb.2009.08.191.

[17] P. Freeman et al., "Recent measurements on MiniMALTA, a radiation hard CMOS sensor with small collection electrodes for ATLAS," in *Proc. Vertex*, Sep. 2020, p. 20, doi: 10.22323/1.373.0020.

[18] H. Pernegger et al., "MALTA-cz: A radiation hard full-size monolithic CMOS sensor with small electrodes on high-resistivity Czochralski substrate," 2023, *arXiv:2301.03912*.